Quantum yields for production of $O(^1D)$ in the ultraviolet photolysis of ozone: Recommendation based on evaluation of laboratory data

Y. Matsumi,[1] F. J. Comes,[2] G. Hancock,[3] A. Hofzumahaus,[4] A. J. Hynes,[5] M. Kawasaki,[6] and A. R. Ravishankara[7]

Received 12 February 2001; revised 13 June 2001; accepted 19 June 2001; published 8 February 2002.

[1] The quantum yield for $O(^1D)$ production in the photolysis of ozone in the ultraviolet region as a function of wavelength and temperature is a key input for modeling calculations in the atmospheric chemistry. To provide the modeling community with the best possible information, the available data are critically evaluated, and the best possible recommendations for the quantum yields are presented. Since the authors of this paper are the principal investigators of the groups which have provided most of the recent experimental data for the $O(^1D)$ quantum yields, the basic assumptions made by each group, the input parameters used in obtaining the quantum yields, and possible sources of systematic errors are well examined. The fitting expression of the $O(^1D)$ yield as a function of photolysis wavelength λ and temperature $T$is presented in the ranges of 306 nm $\leq \lambda \leq$ 328 nm and 200 K $\leq T \leq$ 300 K. The recommendation values of the $O(^1D)$ quantum yield for 290 nm $\leq \lambda \leq$ 306 nm and 328 nm $\leq \lambda \leq$350 nm are also presented. The formation mechanisms of $O(^1D)$ in the photolysis of ozone which result in the wavelength and temperature dependence of the $O(^1D)$ yields are interpreted. *INDEX TERMS:* 0317 Atmospheric Composition and Structure: Chemical kinetic and photochemical properties; 0365 Atmospheric Composition and Structure: Troposphere—composition and chemistry; 0340 Atmospheric Composition and Structure: Middle atmosphere—composition and chemistry; *KEYWORDS:* Ozone, Photolysis, Quantum yield, Ultraviolet, Singlet oxygen atom, atmospheric modeling

1. Introduction

[2] In general, electronically excited species do not play a major role in the chemistry of the Earth's lower atmosphere (i.e., below ~40 km) since they are short-lived owing to collisional deactivation by N_2 and O_2. For this reason, other competing chemical reactions are normally unimportant for such species in the atmosphere. The most notable exception is the first electronically excited state of oxygen atom, $O(^1D)$. $O(^1D)$ is not only metastable (radiative lifetime ~148 s) but also highly reactive toward a number of atmospheric trace gases. The primary reason for the extreme importance of this very low abundant species is that a small fraction of $O(^1D)$ reactions creates highly reactive species from highly unreactive species; this minor pathway for $O(^1D)$ loss is often the major pathway for the generation of the reactive species. Specifically, the OH radical in the stratosphere and troposphere and NO (and eventually all nitrogen oxides) in the stratosphere are produced mostly due to the reactions of $O(^1D)$ with inert H_2O and N_2O.

(R1) $$O(^1D) + H_2O \rightarrow 2OH$$

(R2) $$O(^1D) + N_2O \rightarrow 2NO$$

The reactive species created by these reactions, OH and NO, are immensely important in the atmosphere. (1) OH is the most important initiator of the degradation of the majority of natural and anthropogenic emissions entering the atmosphere. (2) OH reactions provide the pathways that convert chemicals in the atmosphere, sometimes from active to inactive forms and at other times from inactive to active forms. (3) OH is a major catalyst for lower stratospheric ozone removal. (4) Nitric oxide is a crucial ingredient of the stratosphere, and (R2) leads to NO_x ($NO + NO_2$), which is the most important catalyst for ozone destruction in most of the stratosphere. (5) NO_x also suppresses the catalytic destruction of ozone by halogens by sequestering them in unreactive forms such as $ClONO_2$.

[3] The major source of $O(^1D)$ in the lower atmosphere is the photolysis of ozone in the Hartley and Huggins bands. The strong increase in the ozone absorption cross section below 330 nm and the consequent absorption by overhead ozone lead to the sharp decrease of the solar actinic flux, becoming practically 0 below 290 nm in the lower stratosphere and troposphere. Since the photolysis of atmospheric ozone depends on the overlap of the wavelength-dependent actinic flux and on the ozone absorption cross section, the opposing wavelength dependence of these two quantities essentially restricts the photodissociation to ~290–330 nm [*Hofzumahaus et al.*, 1999]. This is precisely the wavelength region where $O(^1D)$ production increases from near-zero values around 330 nm to near-unity values around 290 nm. Therefore the calculated atmospheric $O(^1D)$ production rate is very sensitive to changes in the quantum yield for its production in the photolysis of ozone in this wavelength range. It is also this region where the UV absorption cross sections of ozone and the quantum yields for $O(^1D)$ production are highly sensitive to temperature. Thus accurate definition of the quantum yields for $O(^1D)$ production in ozone photolysis as a function of wavelength and temperature

[1]Solar-Terrestrial Environment Laboratory, Nagoya University, Nagoya, Japan.
[2]Institut für Physikalische und Theoretische Chemie, Johann Wolfgang Goethe Universität, Frankfurt, Germany.
[3]Physical and Theoretical Chemistry Laboratory, Oxford University, Oxford, UK.
[4]Institut für Chemie und Dynamik der Geosphäre, Institut II: Troposphäre, Forschungszentrum Jülich GmbH, Jülich, Germany.
[5]Division of Marine and Atmospheric Chemistry, Rosenstiel School of Marine and Atmospheric Science, University of Miami, Miami, Florida, USA.
[6]Department of Molecular Engineering, Kyoto University, Kyoto, Japan.
[7]NOAA Aeronomy Laboratory, Boulder, Colorado, USA.

0148-0227/02/2001JD000510

is essential for atmospheric chemistry [*Ravishankara et al.*, 1998].

[4] Until a few years ago it was suggested, on the basis of many previous data sets, that the $O(^1D)$ production drops monotonically from near-unity value at ~290 nm to 0 by ~310 nm [*DeMore et al.*, 1994], the threshold for the energetically allowed channel,

$$\text{(R3)} \qquad O_3 + h\nu \rightarrow \quad O(^1D) + O_2(a^1\Delta_g).$$

It was assumed that the spin conservation would require that the coproduct of $O(^1D)$ be $O_2(^1\Delta)$ since the upper state of ozone accessed by absorption in the strongly allowed transition is a singlet. There were, however, some laboratory data that indicated the presence of a "tail" in $O(^1D)$ quantum yield (i.e., a nonzero quantum yield) beyond this threshold [*Brock and Watson*, 1980b; *Trolier and Wiesenfeld*, 1988]. *Adler-Golden et al.* [1982] had pointed out that vibrationally excited ozone could generate $O(^1D)$ via the spin-allowed channel (R3) well beyond the 310-nm energetic threshold calculated for the ground state of ozone, and in contrast to the early NASA/Jet Propulsion Laboratory (JPL) recommendations, an evaluation by *Steinfeld et al.* [1987] recommended a tail in the $O(^1D)$ yield which extended out to 325 nm. *Ball et al.* [1993] reported quantum yield measurements of $O_2(a^1\Delta)$ (the $O(^1D)$ coproduct from the spin-allowed photodissociation of ozone) showing a tail that is very similar to the one for $O(^1D)$ reported previously. *Michelsen et al.* [1994] further developed the concept of *Adler-Golden et al.* [1982] and presented a model calculation that described well the measured tail of the room temperature $O(^1D)$ quantum yield reported by *Brock and Watson* [1980b] and *Trolier and Wiesenfeld* [1988] and $O_2(a^1\Delta)$ reported by *Ball et al.* [1993] up to ~320 nm. Their model assumed that the tail is due only to photolysis of vibrationally excited ozone; it did not take into account the spin-forbidden process, which was not known at that time. Their mathematical expression became the basis for the NASA/JPL recommendation in 1997 [*DeMore et al.*, 1997]. Field experiments that compared $J(O^1D)$ photolysis frequencies measured directly by chemical actinometer with data obtained from solar actinic spectra and $O(^1D)$ quantum yield spectra [*Müller et al.*, 1995; *Shetter et al.*, 1996] were also consistent with the tail. Inclusion of the tail led to a much better agreement between measurements and calculations as a function of solar zenith angle and total overhead ozone column.

[5] The recent laboratory work represented in this paper has yielded new measurements of the $O(^1D)$ quantum yield as a function of wavelength and temperature with direct and indirect detection methods, showing clearly that the tail exists [*Armerding et al.*, 1995; *Takahashi et al.*, 1996a, 1998a; *Ball et al.*, 1997; *Silvente et al.*, 1997; *Talukdar et al.*, 1998; *Bauer et al.*, 2000; *Smith et al.*, 2000]; all groups, except for *Smith et al.* [2000], are represented in this paper. More interestingly, some of these new measurements also show that the quantum yield does not go to 0 even at wavelengths as long as ~330 nm when the temperature is cold enough to eliminate the existence of significant fraction of ozone in its vibrationally excited level. This nonzero yield has been attributed to the spin-forbidden channel for $O(^1D)$ production

$$\text{(R4)} \qquad O_3 + h\nu \rightarrow O(^1D) + O_2\left(X^3\Sigma_g^-\right)$$

and has now been clearly demonstrated via recent laboratory measurements [*Takahashi et al.*, 1996b; *Denzer et al.*, 1997, 1998].

[6] The significance of these changes in $O(^1D)$ quantum yields is very important to atmospheric calculations. *Müller et al.* [1995] have indicated that the tail contributes at least 30% of the noontime $J(O^1D)$ in summer in Jülich (solar zenith angle = 28°) and that total integrated $O(^1D)$ production is enhanced by 1.38 owing to the tail. Furthermore, there are many situations in the atmosphere where the available wavelengths are restricted to >310 nm. Such situations include high solar zenith angles and large overhead ozone columns, both common at high latitudes during late fall to early springtime. Of course, high solar zenith angles occur every day at all sunlit locations at least for a short period. *Talukdar et al.* [1998] suggested that the contributions of the tail and the spin-forbidden dissociation process can make the $J(O^1D)$ value 3 times larger at solar zenith angle of 85° than the value estimated without them.

[7] Currently, the data set for the quantum yields for $O(^1D)$ production in ozone photolysis at wavelengths between ~308 and ~330 nm has not been evaluated. This is because the changes in the quantum yields have been reported only recently and because there still exist significant quantitative differences in the reported values, even though all the recent studies qualitatively substantiate the tail and the existence of the spin-forbidden photodissociation pathway (R4).

[8] To rectify the lack of a good recommendation for the quantum yields for $O(^1D)$ in ozone photolysis, a panel of laboratory scientists and one field measurements scientist working in the area of ozone photodissociation were brought together as a part of the joint Stratospheric Processes and their Role in Climate (SPARC)/International Global Atmospheric Chemistry (IGAC) activity on laboratory studies. This paper is a result of this activity. The aim of this paper is to critically evaluate the data available to date and to develop the best possible data set for atmospheric modeling. To enable in-depth evaluation of the data, the principal investigator(s) from each data set belong to this panel and are authors of this paper (because *Smith et al.* [2000] published their paper after the panel was formed and had already made the preliminary evaluations, they were not represented in this effort). The panel discussed the basic assumptions made by each group, the input parameters such as the absorption cross sections used in obtaining the quantum yields, and possible sources of systematic errors. In addition, a clear choice of a reasonable "anchor" point for the quantum yields allowed renormalization of the data to specific wavelengths. Trends in wavelength dependence of the quantum yields were examined for possible sources of systematic errors and differences. Such critical evaluations are not possible by an outside data panel, which would not have access to much of the needed but unpublished information. Each principal investigator provided such information for this evaluation and enabled a better evaluation where some data could be discarded, corrected, and/or renormalized. This paper lists all the steps and reasons for the choice of data used in this recommendation and the physical basis for the generation of both ground and electronically excited oxygen atoms. Furthermore, a comprehensive easy-to-use equation is employed to represent the best possible data set for atmospheric modeling.

2. Experimental Considerations

[9] The difficulties connected with the measurement of $O(^1D)$ quantum yields from photolysis of ozone are primarily associated with the need for a narrowband, wide tunable source of photolysis radiation, the direct monitoring $O(^1D)$, and the very large dynamic range (especially in ozone cross section) that the measurements span. For a similar photolysis fluence and ozone concentration the concentration of $O(^1D)$ produced varies by six orders of magnitude between 250 and 350 nm. In addition, the lifetime of $O(^1D)$ with respect to either reaction or quenching is extremely short in most common gases; exceptions are gases such as He, Ne, Ar, SF_6, and CF_4.

[10] Most of the experimental data used in producing this evaluation used some type of pulsed tunable laser as the photolysis light source. Such lasers provide a relatively high-power narrow

bandwidth source of tunable radiation. However, the variation in photolysis laser fluence, i.e., energy per unit area (or at least the relative values at different wavelengths), needs to be monitored accurately as the wavelength of the laser changes, and this measurement is not trivial. Since these lasers operate in the visible and require harmonic generation techniques to reach the UV, some changes in beam profile are unavoidable as the lasers are tuned. The recent study by *Smith et al.* [2000] used broadband with bandwidths that varied between 0.05 and 4 nm.

2.1. Direct Techniques for $O(^1D)$ Atom Monitoring

[11] Experimental $O(^1D)$ monitoring techniques are conveniently divided into techniques which monitor $O(^1D)$ directly via spectroscopy or indirectly via approaches which allow the $O(^1D)$ to interact with another gas to produce a species that is more conveniently monitored as a "spectroscopic marker" for $O(^1D)$. $O(^1D)$ can be monitored by its emission $O(^1D) \rightarrow O(^3P)$ at 630 nm. This emission is both spin and electric dipole forbidden with a lifetime of 148 s; nevertheless, direct emission was used to monitor relative $O(^1D)$ quantum yields between 221 and 243.5 nm [*Cooper et al.*, 1993]. It is also possible to monitor $O(^1D)$ in absorption via the 3s $^1D^0{}_2 - 2p^1D_2$ transition at 115.2 nm, and this technique has found limited, and controversial, use in kinetic studies [*Heidner and Husain*, 1973]. It has not been applied to quantum yield measurements. Three approaches using laser excitation have also been published. *Pratt et al.* [1991] reported (2 + 1) resonance-enhanced multiphoton ionization (REMPI) detection of $O(^1D)$ using the $3p^1F_3$ and $3p^1P_1$ transitions at 203.5 and 205 nm. *Richter and Hynes* [1996] reported observation of (3 + 1) REMPI transitions to the $3d^1F_3$ and several other closely spaced levels at ~276 nm. Both sets of REMPI transitions lie within the wavelength region where O_3 absorbs strongly; hence the focused REMPI probe laser generates an interference signal because it produces $O(^1D)$ which it then detects. The (2 + 1) excitation wavelength lies in a minimum in the UV absorption spectrum of O_3 and requires generation of deep UV radiation; however, G. Hancock and coworkers [*Ball et al.*, 1997; *Denzer et al.*, 1997, 1998] have successfully applied it to $O(^1D)$ yield measurements between 305 and 330 nm. The (3 + 1) wavelength, 276 nm, is easily generated using currently available tunable lasers, but this excitation wavelength lies close to the peak in the ozone absorption cross section. Hence background interferences are sufficiently severe that this detection scheme has little utility for yield studies at long wavelengths. Finally, laser-induced fluorescence (LIF), using single photon excitation of the $3s^1D^0{}_2 - 2p^1D_2$ transition, has been demonstrated by *Takahashi et al.* [1996a, 1996b, 1997, 1998a]. This is technically the most demanding approach, requiring sum frequency generation of vacuum ultraviolet (VUV) radiation with two tunable lasers. Nevertheless, it appears to offer high sensitivity, specificity, and no significant interference effects.

[12] Potential complications from the use of direct laser-based detection techniques can arise when they are used in conjunction with another laser to photolyze ozone. The first of these arises because a polarized detection laser excites a subset of the magnetic sublevels of $O(^1D)$. In the absence of an electric or magnetic field these levels are degenerate and equally populated. However, a polarized laser may produce a preferential population in some of these sublevels; thus "an orbital alignment effect" can occur. If the "alignment effect" varies as the photolysis wavelength is changed, the probe laser signal may not reflect the overall atomic production rate. A second complication occurs when the atom is produced with a large amount of translational energy, such that its Doppler line width exceeds that of the probe laser. Again, the laser excites only a subset of the atoms, those whose velocities match the excitation laser profile. It is important to note that the presence of these effects will not necessarily cause errors in a relative yield measurement and may also be present in the indirect detection schemes. However, if the population of the levels that are monitored changes in a manner which does not reflect the total change in population as a function of photolysis wavelength, errors will occur. Orbital alignment effects have been seen in the production of $O(^1D)$ from the photolysis of N_2O [*Suzuki et al.*, 1996; *Ahmed et al.*, 1999; *Neyer et al.*, 1999]; however, such effects seem to be either absent or not to affect yield measurements in O_3 photolysis. Effects of changes in the Doppler profile of $O(^1D)$ will depend on the bandwidth of the excitation laser. *Takahashi et al.* [1998a] found that it was necessary to correct their $O(^1D)$ yield measurements by up to 50% to compensate for Doppler broadening at the longest wavelengths at which they made measurements, whereas *Ball et al.* [1997] concluded that their measurements were unaffected by such effects.

2.2. Indirect Techniques for $O(^1D)$ Atom Monitoring

[13] Because of the difficulties associated with direct observation of $O(^1D)$ many studies have utilized indirect detection, allowing the $O(^1D)$ to react with another molecule which is more easily monitored. Clearly, the disadvantage of this approach is that it is indirect and that $O(^1D)$ production is inferred. In this case, knowledge of the detailed chemistry associated with production of the "spectroscopic marker" is desirable and may be obtained by careful variations in experimental conditions. Several studies have photolyzed O_3 in the presence of N_2O. The reaction of $O(^1D)$ with N_2O produces NO, which then undergoes further reaction with ozone, producing electronically excited NO_2* that can be detected by its chemiluminescence. It is very difficult to quench vibrationally hot NO by bath gases that do not also quench $O(^1D)$. The kinetics of this system are complicated by the fact that NO is produced with a great deal of vibrational excitation, and this appears to enhance the rate of its reaction with ozone. This approach was used in several early studies [*Kuis et al.*, 1975; *Moortgat and Warneck*, 1975; *Philen et al.*, 1977; *Arnold et al.*, 1977; *Fairchild and Lee*, 1978; *Brock and Watson*, 1980b], including two which used tunable laser photolysis and which failed to report the tail in the $O(^1D)$ yield. *Smith et al.* [2000] also used this approach, with the exception that they used chemical ionization mass spectrometry (CIMS) for detection of the product NO_2. *Brock and Watson* [1980b] used laser photolysis in the first published study which reported the existence of the tail, while *Smith et al.* [2000] used broadband photolysis and again reported observation of the tail; thus it appears that neither the chemistry of the $N_2O/O(^1D)$ system nor the mode of photolysis is responsible for the failure of early studies to observe the tail. *Trolier and Wiesenfeld* [1988] used energy transfer from $O(^1D)$ to CO_2 followed by detection of the infrared emission from vibrationally excited CO_2. More recently, three groups have monitored the OH produced by the reaction of $O(^1D)$ with water, H_2, or methane. $O(^1D)$ reacts at close to gas kinetic rates with hydrides with a well-understood chemistry. Furthermore, H_2O is very efficient at quenching vibrationally excited OH and does not "react" with vibrationally excited OH. Each study utilized LIF to monitor the OH, although they used different excitation schemes. *Talukdar et al.* [1998] excited the *A-X* (1-0) transition at 282-nm monitoring (1-1) and (0-0) fluorescence at 308–315 nm. This detection scheme discriminates effectively against scattered probe laser light. Since the excitation transition lies within the absorption spectrum of ozone, the probe beam generates some $O(^1D)$ atoms which can react within the time frame of the probe pulse to generate an interfering OH LIF signal. This increases the background or "noise" signal relative to the LIF signal from OH produced by the photolysis laser but introduces no complications. *Armerding et al.* [1995] monitored the formation of OH in its ground vibrational level exciting the *A-X* (0-0) transition at 308 nm; in this scheme, OH interference is reduced substantially, but the excitation and detection wavelengths are similar. Noise from the detection of scattered probe light is the main factor limiting detection sensitivity. The reaction of $O(^1D)$ with H_2 and CH_4produces OH with a substantial amount of vibrational excitation. *Silvente et al.* [1997] and *Bauer et al.* [2000] monitored OH ($\nu = 1$) by exciting the *A-X*

Table 1. Experimental Data of Absolute $O(^1D)$ Quantum Yield $\Phi(^1D)$ in the Photolysis of O_3 at 308 nm at Room Temperature

$\Phi(^1D)$	Uncertainty	Reference	Method
0.79	±0.10	*Talukdar et al.* [1997]	time profile of $O(^3P)$ resonance flourescence intensity
0.79	±0.12	*Takahashi et al.* [1996b]	photofragment yield spectra of $O(^3P)$ and $O(^1D)$ by VUV-LIF
0.79	±0.02	*Greenblatt and Wiesenfeld* [1983]	time profile of $O(^3P)$ resonance fluorescence intensity

(0-1) transition at 351 nm and monitoring blue shifted fluorescence at 308 nm. This approach minimizes noise and OH interference effects and allowed *Bauer et al.* [2000] to monitor $O(^1D)$ yields out to 375 nm. This scheme assumes that the internal state distribution of the OH does not change with photolysis wavelength. If the translational energy of $O(^1D)$ varied as a function of photolysis wavelength and this were to change the internal state distribution of OH, it would be a problem. *Bauer et al.* [2000] monitored OH formation in relatively high pressures of He such that $O(^1D)$ should have been translationally thermalized. *Silvente et al.* [1997] monitored OH produced by $O(^1D)$ that was much closer to the nascent translational distribution. In addition, *Bauer et al.* [2000] used both $H_2$and CH_4 as reactant hydrides and obtained identical results suggesting that this is not a significant problem.

[14] As noted above, *Smith et al.* [2000] used a combination of a monochromator and a Xe arc lamp for photolysis of N_2O/O_3 mixtures with CIMS detection of the NO_2 product. The NO molecule reacts with the O_3 and then produces NO_2. The NO_2 is ionized by an ion-molecule reaction with O_3^-. Finally, the NO_2^- ion is detected with a quadrupole mass spectrometer. This method can distinguish $O(^1D)$ from $O(^3P)$ without using any laser system. Also, unlike the previous studies that utilized the $O(^1D) + N_2O$ reaction, vibrationally excited NO should not be a problem since $NO_2$was detected directly and all of the NO (ground and vibrationally excited) was converted rapidly to NO_2. Their observation of the tail confirms that this is not an artifact produced by the high peak power associated with laser photolysis. However, they used large bandwidths for the photolysis light (0.1–3.6 nm, full width at half maximum (FWHM)), while the bandwidths in the laser experiments are much narrower (<0.01 nm). The high-resolution $O(^1D)$ quantum yield data [*Takahashi et al.*, 1996a, 1998a; *Bauer et al.*, 2000] show variations on a much finer scale than the bandwidths used by *Smith et al.* [2000]. This implies that the yield values for the specific wavelengths presented by *Smith et al.* [2000] may have problems if the quantum yield varies significantly within their detection bandwidth. Therefore the yield for a given wavelength presented by *Smith et al.* [2000] is a weighted average for a wavelength that should account for the variation of the absorption cross section of ozone and $O(^1D)$ quantum yield in ozone photodissociation.

2.3. Other Experimental Factors

[15] While the convergence of recent measurements is gratifying, significant and puzzling discrepancies remain even between the various studies used in this recommendation. No obvious single experimental factor seems to emerge as the culprit. The discrepancies that remain are significant, and further studies to resolve them are required. In the opinion of the authors the variation of the photolysis fluence coupled with changes in beam profile with changes in wavelength remains a significant potential source of systematic error in such measurements.

[16] The power meters used by a Japanese group [*Takahashi et al.*, 1996a, 1998a] and a National Oceanic and Atmospheric Administration (NOAA) group [*Talukdar et al.*, 1998] were intercompared to test if the measurements of relative laser fluence as a function of wavelength were a source of error (details of this intercomparison are available at http://www.sparc.sunysb.edu/html/RefData.html). First, the NOAA power meter was calibrated at 248 nm relative to the National Institute of Standards and Technology (NIST) standard. This calibration showed that the power meter was accurate to better than 3% at 9 m J pulse^{-1}(close lose to the values used in NOAA studies) and to better than ~7% at 0.5 m J pulse^{-1}. Second, the Japanese power meter was compared with the NOAA power meter at 351 nm and found to respond linearly with laser energy but with a relative response that differed by ~10%. Third, the Japanese and NOAA power meters were intercompared at 248, 282, and 308 nm. The responses of both power meters were linear and again differed by ~9% at all wavelengths. Therefore it is safe to assume that there was no systematic difference in the measurement of the laser fluence as a function of wavelength in these two power meters over the range of wavelengths used for $O(^1D)$ quantum yields discussed here. Although we have not measured the relative response at every wavelength used or intercompared the power meters used by all the groups, they should not be different because of the principle of operation of these power meters. Furthermore, the normalization of the quantum yield data to 308 nm removes the differences in response on an absolute scale. The relative response as a function of wavelength could still contribute to the uncertainty, but this contribution cannot be more than 15–20% on the basis of the experience with the two power meters discussed above. Such possible differences in the response are included in the estimation of the uncertainties in the evaluated values.

3. Data Treatment and Recommendations

[17] The recommendations for the $O(^1D)$ quantum yields in the photolysis of O_3 were derived using the following procedures. First, on the basis of data from the studies considered here the quantum yield of $O(^1D)$ at 298 K at 308 nm was set to 0.79. Second, we derived a wavelength dependence of quantum yields at 298 K between 306 and 328 nm by checking and renormalizing the experimental data presented by several groups and then averaging them. The wavelength dependence at 298 K was also anchored at 308 nm. Third, we determined the parameters in the chosen expression (see section 3.3) for 306 nm $< \lambda <$ 328 nm and 200 K $< T <$ 320 K by fitting the temperature-dependent yields obtained above to this expression. All the data used in this evaluation are available as supplementary material and can be accessed from the SPARC Data Center web site (http://www.sparc.sunysb.edu/html/RefData.html).

3.1. Absolute Quantum Yield at 308 nm at Room Temperature

[18] There are several absolute measurements of $O(^1D)$ quantum yields in the photolysis of ozone at 248, 266, and 308 nm [*Talukdar et al.*, 1997; *Takahashi et al.*, 1996a, 1998a; *Greenblatt and Wiesenfeld*, 1983; *Amimoto et al.*, 1980]. Since the photolysis of ozone at wavelengths longer than 300 nm is of importance in atmospheric chemistry, the absolute measurements at 308 nm are most important among those studies. Table 1lists the results of the absolute measurements at 308 nm. Two types of experimental method were used for the measurements of the absolute yield. *Talukdar et al.* [1997] and *Greenblatt and Wiesenfeld* [1983]

measured the time profile of $O(^3P)$ resonance fluorescence after the pulsed laser photodissociation of O_3. The temporal profile of $O(^3P)$ initially jumps due to the direct formation in the photolysis of O_3, followed by an exponential rise controlled by the following reactions of $O(^1D)$ and a slow decay due to diffusion.

$$\text{(R5)} \qquad O(^1D) + O_3 \rightarrow 2O_2,$$

which is rate coefficient k_5, and

$$\text{(R6)} \qquad O(^1D) + O_3 \rightarrow 2O(^3P) + O_2,$$

which is rate coefficient k_6. The absolute $O(^1D)$ quantum yield value was calculated from amounts of the initial jump and the exponential rise of the $O(^3P)$ signal on the basis of experimental results that the two rate coefficients are equal ($k_5/k_6 = 1.0$) [*DeMore et al.*, 1997; *Talukdar et al.*, 1997]. Although both groups used XeCl excimer laser light as a light source at 308 nm, we estimate that the difference is <1% from the usage of a monochromatic light at 308.0 nm. However, *Takahashi et al.* [1996a, 1998a] measured photofragment yield spectra of both $O(^3P)$ and $O(^1D)$ after the photolysis of O_3 by scanning the photolysis laser wavelength between 308 and 326 nm and by monitoring the $O(^3P)$ and $O(^1D)$ concentration with a VUV laser-induced fluorescence technique. The sum of the photofragment yield spectra for both $O(^1D)$ and $O(^3P_j)$ atoms with absolute scales should correspond to the absorption spectrum (ABS) of the O_3 molecule

$$\sigma_{ABS}(\lambda) = s_{1D}Y_{1D}(\lambda) + s_{3P}Y_{3P}(\lambda), \qquad (1)$$

where $\sigma_{ABS}(\lambda)$ is the absorption spectrum of O_3 at wavelength λ, $Y_{1D}(\lambda)$ and $Y_{3P}(\lambda)$ are the experimentally obtained photofragment yield spectra of $O(^1D)$ and $O(^3P_j)$, and s_{1D} and s_{3P} are the detection sensitivity factors for $O(^1D)$ and $O(^3P_j)$, respectively. Since the yield spectra of $O(^1D)$ and $O(^3P)$ are not parallel in the wavelength range of 308–328 nm, a pair of the s_{1D} and s_{3P} values were determined so that the sum of $s_{1D}Y_{1D}(\lambda)$ and $s_{3P}Y_{3P}(\lambda)$ reproduced the absorption spectrum $\sigma_{ABS}(\lambda)$. The absolute value of $O(^1D)$ quantum yield is calculated as $\Phi(\lambda) = s_{1D}Y_{1D}(\lambda)/\sigma_{ABS}(\lambda)$.

[19] As listed in Table 1, the published absolute values for the $O(^1D)$ quantum yield S at 308 nm are in good agreement with each other in spite of using the two different experimental techniques. We adopted the value of 0.79 for the $O(^1D)$ yield at 308 nm at room temperature as a standard ("anchor") point. The quoted uncertainty is in the range of 0.02–0.12 from the value at this point (Table 1) from the different studies. The value of 0.02 for the uncertainty estimated by *Greenblatt and Wiesenfeld* [1983] seems to be too small because the uncertainty of the assumption of $k_5/k_6 = 1.0$ should be >2–3%. Additional work to determine more accurately the absolute value of $O(^1D)$ quantum yield at 308 nm is needed since this value affects the overall accuracy of the yields at other wavelengths.

3.2. $O(^1D)$ Quantum Yield at 298 K in the Wavelength Range of 306–328 nm

[20] There are many studies on the quantum yields between 306 and 328 nm at room temperature (298 K). To obtain a wavelength dependence of the $O(^1D)$ yield at 298 K in the wavelength range of 306–328 nm, the recent experimental data sets reported by eight groups are used [*Talukdar et al.*, 1998; *Takahashi et al.*, 1996a; *Ball et al.*, 1997; *Armerding et al.*, 1995; *Bauer et al.*, 2000; *Brock and Watson*, 1980b; *Trolier and Wiesenfeld*, 1988; *Smith et al.*, 2000]. In these studies the existence of the tail around 315 nm is obvious. The wavelength dependencies measured by the different laboratories look quite similar, but there are some differences among the reported values of the quantum yields. In these studies the relative $O(^1D)$ concentrations were measured at various wavelengths for O_3 photolysis, for example, by detecting the laser-induced fluorescence intensity of OH radical produced by the reaction $O(^1D) + H_2O \rightarrow 2OH$. Then the relative $O(^1D)$ concentration obtained at each photolysis wavelength was divided by a value of the published absorption cross section. In most of the recent studies [*Talukdar et al.*, 1998; *Ball et al.*, 1997; *Armerding et al.*, 1995; *Bauer et al.*, 2000] the absorption cross sections reported by *Malicet et al.* [1995] were used to calculate relative quantum yields. *Trolier and Wiesenfeld* [1988] used the absorption data reported by *Molina and Molina* [1986]. *Smith et al.* [2000] also used the absorption data by *Molina and Molina* [1986] but included the as-yet-unpublished higher-resolution data from their laboratory. *Brock and Watson* [1980b] used absorption cross sections measured by *Moortgat and Warneck* [1975]. The difference between the two sets of absorption data from *Malicet et al.* [1995] and *Molina and Molina* [1986] is small (<2%) in the wavelength range of 306–316 nm and is <6% between 317 and 328 nm. The choice between the two absorption data sets does not lead to a large error in the calculation of the $O(^1D)$ quantum yields. However, we have recalculated the quantum yield data obtained from relative measurements by *Brock and Watson* [1980b] using the absorption cross sections by *Malicet et al.* [1995] since the absorption cross sections which *Brock and Watson* [1980b] originally used differ from the recent two absorption data.

[21] We have renormalized the data sets to reduce the systematic error before averaging them. The renormalization factors for the data sets were chosen to achieve the best consistency among the yield curves over the full 307–320 nm wavelength range. The average of the renormalized data set was scaled to have the value of 0.79 at 308 nm, which is the standard point we employed. Table 2 lists the renormalization factors, the renormalized $O(^1D)$ yield data sets of the eight groups, and their average values. It should be noted that the data set reported by *Takahashi et al.* [1996a] is not renormalized since they used an absolute method to obtain the yield value as described in section 3.1. The highly wavelength-resolved data of *Takahashi et al.* [1996a] were binned into 1-nm intervals in this calculation. In the averaging of the values at 308 nm the extremely large value reported by *Ball et al.* [1997] was excluded. We have checked experimental results reported by others in addition to the eight groups. Since those results had exceedingly different wavelength dependence from the data sets by the eight groups, we omitted those data in the calculation to obtain the quantum yields at 298 K in the wavelength range of 306–328 nm. The renormalized values of the data sets reported by the eight groups and their average values are plotted in Figure 1. The absorption cross sections at 295 K reported by *Malicet et al.* [1995] are also listed in Table 2 and were used to calculate the absolute quantum yields from the relative measurements of $O(^1D)$ concentrations in the studies by *Talukdar et al.* [1998], *Ball et al.* [1997], *Armerding et al.* [1995], and *Bauer et al.* [2000]. The differences of the absorption cross sections between 295 and 298 K are estimated to be negligibly small (<2%).

[22] We used 1.0-nm intervals for the derived quantum yields at 298 K, and later we also used 1.0-nm intervals in the calculation of the fitting expression for the temperature dependence. The 1.0-nm intervals seem insufficient to resolve the fine structures in the ozone absorption spectrum. There is some evidence for structure between 312 and 320 nm, which can be seen in the high-resolution quantum yield spectrum of $O(^1D)$ reported by *Takahashi et al.* [1996a]. The 1-nm intervals are also insufficient to resolve the structure in a solar actinic flux spectrum. However, *Hofzumahaus et al.* [1999] have shown that the calculation of $J(O^1D)$ (photolysis frequency of O_3 to form $O(^1D)$) using 1-nm resolution is <2% different from the higher-resolution calculation even at solar zenith angles below 80°. Therefore we believe that the 1-nm resolution is sufficient for current atmospheric calculations.

Table 2. $O(^1D)$ Quantum Yields in the Photolysis of O_3 Between 306 and 328 nm at 298 K[a]

λ, nm	*Talukdar et al.* [1998][b]	*Takahashi et al.* [1996a][b]	*Ball et al.* [1997][c]	*Armerding et al.* [1995][d]	*Bauer et al.* [2000][e]	*Brock and Watson* [1980b][f]	*Trolier and Wiesenfeld* [1988][g]	*Smith et al.* [2000][b]	Average[h]	Fitting Results[i]	JPL 1997[j]	IUPAC 1997[k]	Abs., [l] cm^2
306	0.85	0.85	0.89		0.86	1.02	0.90	0.84	0.884	0.884	0.908	0.950	1.76E-19[m]
307	0.85	0.84	0.89	0.87	0.83	0.92	0.91	0.80	0.862	0.862	0.851	0.877	1.54E-19
308	0.78	0.79		0.83	0.81	0.80	0.73	0.79	0.790	0.793	0.740	0.773	1.35E-19
309	0.67	0.71	0.75	0.72	0.62	0.66	0.66	0.70	0.683	0.671	0.605	0.677	1.24E-19
310	0.55	0.56	0.60	0.51	0.40	0.53	0.52	0.62	0.534	0.523	0.476	0.600	1.02E-19
311	0.40	0.42	0.39	0.42	0.32	0.41	0.37	0.44	0.395	0.394	0.380	0.388	9.18E-20
312	0.33	0.35	0.30	0.32	0.26	0.31	0.31	0.35	0.316	0.310	0.315	0.303	7.87E-20
313	0.27	0.32	0.26	0.24	0.24	0.27	0.29	0.34	0.278	0.265	0.280	0.262	6.80E-20
314	0.22	0.30	0.22	0.22	0.22	0.23	0.29	0.27	0.245	0.246	0.265	0.238	6.29E-20
315	0.21	0.29		0.23	0.24	0.24	0.25	0.22	0.240	0.239	0.263	0.235	5.10E-20
316	0.25	0.27	0.21	0.21	0.22	0.23	0.22	0.28	0.236	0.233	0.237	0.221	4.66E-20
317	0.23	0.26		0.21	0.22	0.20	0.23	0.26	0.230	0.222	0.212	0.209	4.12E-20
318	0.19	0.23	0.18	0.16	0.21		0.21	0.24	0.203	0.206	0.203	0.194	3.70E-20
319	0.21	0.26		0.14	0.22		0.20	0.27	0.217	0.187	0.223	0.178	2.71E-20
320	0.15	0.21	0.12	0.13	0.15	0.12	0.19	0.19	0.157	0.166	0.090	0.148	3.25E-20
321	0.14	0.20			0.14		0.09	0.17	0.148	0.146	0.067	0.121	2.00E-20
322	0.11	0.15	0.11		0.11			0.15	0.126	0.128	0.031	0.097	2.42E-20
323	0.09	0.13			0.09			0.13	0.110	0.113	0.043	0.092	1.96E-20
324	0.08	0.13	0.09		0.09			0.13	0.104	0.101	0.037	0.080	1.20E-20
325	0.09	0.10		0.06	0.08	0.05	0.07	0.11	0.080	0.092	0.010	0.070	1.73E-20
326	0.09	0.11	0.13		0.08			0.10	0.101	0.086			1.11E-20
327	0.09	0.12			0.07			0.10	0.093	0.082			8.38E-21
328	0.08	0.09	0.11		0.06			0.12	0.093	0.080			1.30E-20

[a] The renormalized values of the results reported by eight groups and the average values are listed.
[b] A renormalization factor of 1.00 was used in this work.
[c] A renormalization factor of 0.93 was used in this work. Data point at 308 nm has been excluded as an outlier.
[d] A renormalization factor of 1.05 was used in this work. Data points at 327.5 and 330 nm have been excluded owing to their very large errors bars (56% and 72%, respectively).
[e] A renormalization factor of 1.03 was used in this work.
[f] A renormalization factor of 1.05 was used in this work. Data reported by *Brock and Watson* [1980b] have also been recalculated with respect to the absorption cross section, as described in section 2.2.
[g] A renormalization factor of 0.93 was used in this work.
[h] Average of the values from the eight groups.
[i] Value is calculated with (3) and parameter values in Table 3.
[j] See *DeMore et al.* [1997].
[k] See *Atkinson et al.* [1997].
[l] Absorption cross sections of O_3 at 295 K. Taken from *Malicet et al.* [1995].
[m] Read 1.76E-19 as 1.76×10^{-19}.

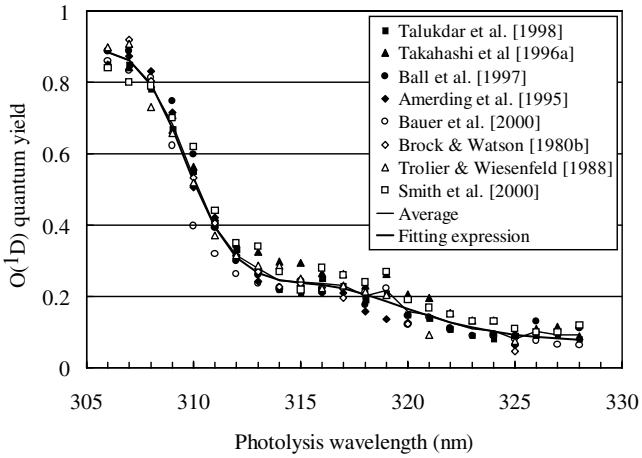

Figure 1. Wavelength dependence of the $O(^1D)$ quantum yield in the photolysis of O_3 at 298 K. The renormalized values of the data sets reported by eight groups [*Talukdar et al.*, 1998; *Takahashi et al.*, 1996a; *Ball et al.*, 1997; *Armerding et al.*, 1995; *Bauer et al.*, 2000; *Brock and Watson*, 1980b; *Trolier and Wiesenfeld*, 1988; *Smith et al.*, 2000] and their average values are plotted. The recommendation values calculated with (3) for 298 K is also plotted.

[23] The accuracy of the photolysis wavelength should be also considered. It has been indicated that a wavelength shift of only 0.1 nm would add another systematic difference of 2–3% in the calculated $J(O^1D)$, even if the actinic flux spectrum is recorded with a bandpass of 1.0 nm [*Hofzumahaus et al.*, 1999]. Wavelengths in this paper are expressed by the values in air (not in vacuum) as wavelength values in air were used in the reports of the O_3 absorption cross section [*Molina and Molina*, 1986; *Malicet et al.*, 1995].

3.3. Temperature Dependence of the Quantum Yield

[24] To obtain the parameters for the expression to calculate the recommended values in the ranges of T = 200–320 K and λ = 306–328 nm, we have used the experimental data of the temperature dependence reported by *Talukdar et al.* [1997, 1998], *Takahashi et al.* [1998a], *Hancock and Hofzumahaus* [1997], *Bauer et al.* [2000], and *Smith et al.* [2000] as well as the averaged data at 298 K described above. First, the temperature dependence of the $O(^1D)$ yield at 308 nm was examined. In the first approximation it was assumed that the $O(^1D)$ quantum yield linearly depends on temperature. The linear least squares fitting to the detailed experimental results at 308 nm, assuming a quantum yield of 0.79 at 298 K, leads to the equation

$$\Phi(308\ \text{nm}, T) = 6.10 \times 10^{-4} T + 0.608\,, \qquad (2)$$

where T is temperature (in K). Figure 2 shows the plots of

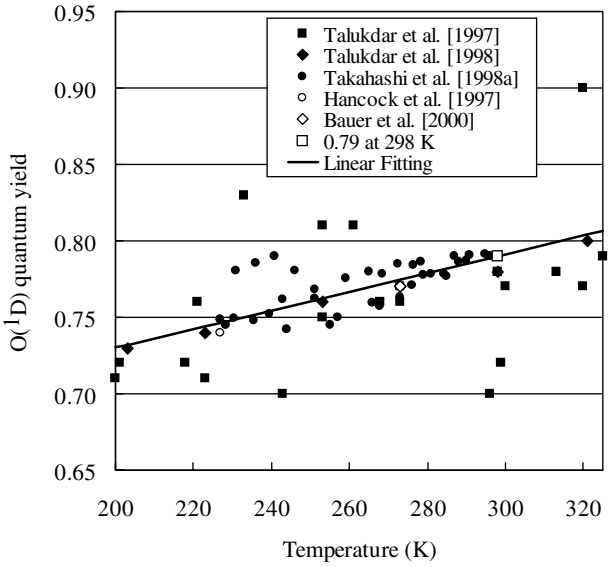

Figure 2. Temperature dependence of the O(^1D) quantum yield in the photolysis of O_3 at 308 nm. The experimental results reported by *Talukdar et al.* [1997, 1998], *Takahashi et al.* [1998a], *Hancock and Hofzumahaus* [1997], and *Bauer et al.* [2000] are plotted. The straight line indicates the results of the linear least squares fitting under the condition of the fixed point of 0.79 at 298 K, (2) in the text.

experimental results of the O(^1D) quantum yield at 308 nm versus temperature and also shows the fitting results of (2). The experimental data at temperatures other than 298 K, reported by the above five groups, are normalized to Φ(308 nm), calculated from this expression. Again, the data at 228 K by *Takahashi et al.* [1998a] were not renormalized since they used an absolute method to obtain the yield value. Figure 3 shows the renormalized values of the quantum yield data at and near 227 K, the original data of which were obtained by *Takahashi et al.* [1998a] and *Hancock and Hofzumahaus* [1997] at 227 K, *Talukdar et al.* [1998] at 223 K, and *Smith et al.* [2000] at 226 K.

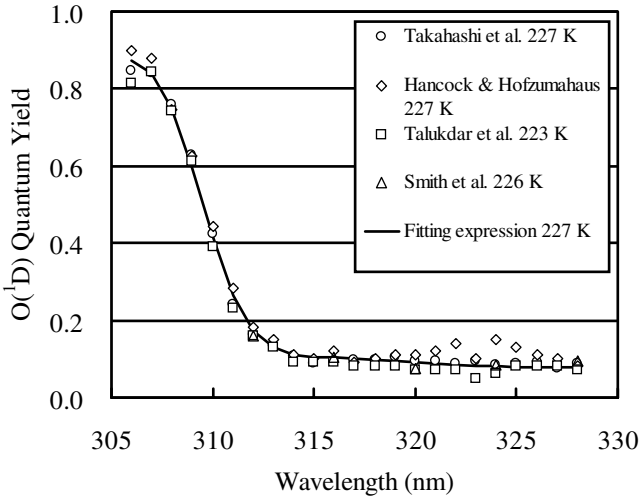

Figure 3. Wavelength dependence of the O(^1D) quantum yield in the photolysis of O_3 at and near 227 K. The renormalized values of the data sets are plotted, the original data of which were obtained by *Takahashi et al.* [1998a] and *Hancock and Hofzumahaus* [1997] at 227 K, *Talukdar et al.* [1998] at 223 K, and *Smith et al.* [2000] at 226 K. Solid line indicates the recommendation curve calculated with (3) for 227 K.

[25] For the fitting expression an equation containing three Gaussian-like functions, a temperature term, and a constant term was used

$$\Phi(\lambda, T) = \left(\frac{q_1}{q_1+q_2}\right)A_1 \exp\left[-\left(\frac{X_1-\lambda}{\omega_1}\right)^4\right] + \left(\frac{q_2}{q_1+q_2}\right)A_2\left(\frac{T}{300}\right)^2 \cdot \exp\left[-\left(\frac{X_2-\lambda}{\omega_2}\right)^2\right] + A_3\left(\frac{T}{300}\right)^{1.5}\exp\left[-\left(\frac{X_3-\lambda}{\omega_3}\right)^2\right] + c, \quad (3)$$

where

$$q_i = \exp\left(-\frac{\nu_i}{RT}\right), \quad (4)$$

and X_{1-3}, A_{1-3}, ω_{1-3}, ν_2, and c are fitting parameters, λ is given in nanometers and T is given in degrees kelvin, and values of ν_1 and R are 0 (cm^{-1}) and 0.695 (cm^{-1} K^{-1}), respectively. This expression has some physical basis. The constant term c is included to represent the spin-forbidden channel and is assumed to be wavelength and temperature independent It is assumed to be temperature independent since we expect this channel to be occurring from the ground state of O_3. It is assumed to be wavelength independent because there are no data to support either wavelength-dependent structure or variation. The first rapidly dropping function is supposed to represent the spin-allowed channel from the ground vibrational state of O_3. The second and third terms represent the dissociation from the vibrationally excited states. The need for two terms is clear in reproducing observed quantum yields. The (T/300) term was needed to adequately fit the data. Furthermore, the expressions derived on a physical basis by *Adler-Golden et al.* [1982] and *Michelsen et al.* [1994] did not fit the data as well as (3). It should be noted that once the complete mechanism for ozone photodissociation and UV absorption by ozone is understood, a more physically based model can be derived. Evidence for these processes and the possible reasons for their origin are given in section 4. However, the rigorous consideration of the physical mechanisms may make the calculation processes of Φ(λ, T) too complicated to use in practical models [*Taniguchi et al.*, 2000].

[26] The values of the parameters were obtained by fitting the expression to the data using a nonlinear least squares method. In the least squares calculation the weight of the average data at 298 K was set to 8, while those of the other individual data were 1. The obtained best fit parameters are listed in Table 3. We recommend the values calculated using (3) and parameters in Table 3 for the O(^1D) quantum yields in the wavelength range of 306 nm < λ < 328 nm and in the temperature range of 200 K < T < 320 K. Table 4 lists the calculated quantum yields at various temperatures and various wavelengths using (3) and the parameter values in Table 3. The calculated yield curves at the temperatures of 298 K and 227 K are plotted in Figures 1 and 3, respectively, for comparison with the experimental data.

[27] The comparisons of the values calculated at 298 K using the expressions in this work and JPL 1994 [*DeMore et al.*, 1994], JPL 1997 [*DeMore et al.*, 1997], and JPL 2000 [*Sander et al.*, 2000] recommendations are shown in Figure 4. Between 307 and 325 nm the results of this work and the JPL 2000 recommendations at 298 K

Table 3. Parameters for (3) to Calculate Recommendation Values of O(^1D) Quantum Yields

	i = 1	i = 2	i = 3
X_i, nm	304.225	314.957	310.737
ω_i, nm	5.576	6.601	2.187
A_i	0.8036	8.9061	0.1192
ν_i, cm^{-1}	0	825.518	
c	0.0765		

Table 4. Recommendation Values of the O(^1D) Quantum Yields in the Photolysis of O_3 at Various Temperatures Calculated with (3) and the Parameters in Table 3

Wavelength, nm	321 K	298 K	273 K	253 K	223 K	203 K
306	0.893	0.884	0.878	0.875	0.872	0.872
307	0.879	0.862	0.850	0.844	0.838	0.836
308	0.821	0.793	0.772	0.760	0.748	0.744
309	0.714	0.671	0.636	0.616	0.595	0.585
310	0.582	0.523	0.473	0.443	0.411	0.396
311	0.467	0.394	0.334	0.298	0.259	0.241
312	0.390	0.310	0.246	0.208	0.169	0.152
313	0.349	0.265	0.200	0.162	0.126	0.112
314	0.332	0.246	0.180	0.143	0.108	0.095
315	0.325	0.239	0.173	0.136	0.102	0.090
316	0.317	0.233	0.168	0.133	0.100	0.088
317	0.300	0.222	0.162	0.129	0.098	0.087
318	0.275	0.206	0.152	0.123	0.096	0.086
319	0.246	0.187	0.141	0.116	0.093	0.085
320	0.214	0.166	0.129	0.109	0.090	0.083
321	0.183	0.146	0.117	0.101	0.087	0.082
322	0.155	0.128	0.107	0.095	0.084	0.080
323	0.132	0.113	0.098	0.089	0.082	0.079
324	0.114	0.101	0.091	0.085	0.080	0.078
325	0.101	0.092	0.086	0.082	0.079	0.078
326	0.091	0.086	0.082	0.080	0.078	0.077
327	0.085	0.082	0.080	0.079	0.077	0.077
328	0.081	0.080	0.078	0.078	0.077	0.077

are in good agreement with each other. It should be noted that the JPL 2000 recommendations were based partly on the previous discussions of our panel in progress. The O(^1D) quantum yield values calculated using (3) and parameters in Table 3 for 298 K, 253 K, and 203 K are plotted in Figure 5.

[28] We also tried to use linear polynomial functions up to sixth order for temperature and sixth order for wavelength in a similar way used in the JPL 1994 recommendation [*DeMore et al.*, 1994]. However, even the 6 × 6 orders function with 49 adjustable parameters did not reproduce the experimental results as well as the above expression in the wavelength range of 306–328 nm.

[29] The primary uncertainties of our recommendation values come from the absolute value at 308 nm which we employed as an "anchor" point (Table 1). Then the relative measurements for the wavelength and temperature dependence give some errors. The fitting of (3)to the experimentally obtained values also produces some errors. At room temperature (298 K) we estimate the uncertainties of the quantum yield values calculated with (3) are ±10% (1σ) for $\Phi(\lambda, 298\ K) \geq 0.4$, while the uncertainties are estimated to be ±0.04 in the absolute value for $\Phi(\lambda, 298\ K) < 0.4$. At temperatures other than room temperature the uncertainties of the yield are estimated to be ±15% for $\Phi(\lambda, T) \geq 0.4$ and ±0.06 for $\Phi(\lambda, T) < 0.4$.

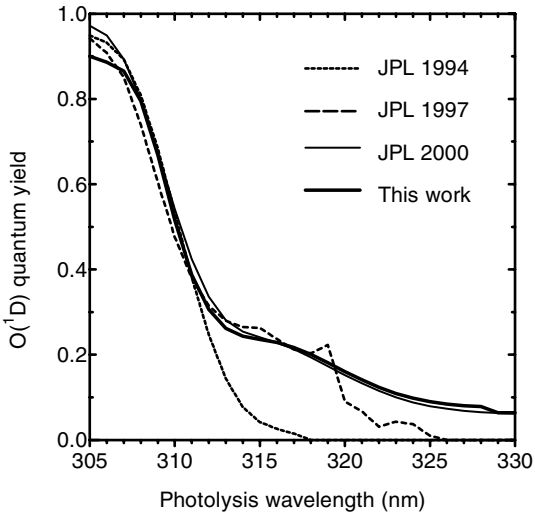

Figure 4. Comparison of the recommendation values of O(^1D) quantum yields at 298 K in the wavelength range 305–330 nm from this work ((3)with the fitting parameters in Table 3), JPL 1994 [*DeMore et al.*, 1994], JPL 1997 [*DeMore et al.*, 1997], and JPL 2000 [*Sander et al.*, 2000].

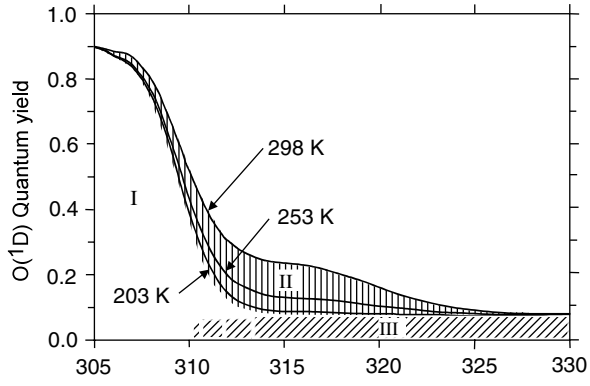

Figure 5. Recommendation values of O(^1D) quantum yields calculated with (3) and the fitting parameters in Table 3 for 203, 253, and 298 K in the wavelength range 305–330 nm (solid lines). Contributions made by the various dissociation processes to the quantum yields for O(^1D) atoms from O_3 photolysis are also indicated. Region I corresponds to the O(^1D) formation following excitation of parent vibration less molecules and dissociation via channel (R3), O(^1D) + $O_2(a^1\Delta_g)$. Region II (vertical hatching) indicates the contribution from the hot-band excitation process leading to O(^1D) formation via channel (R3), O(^1D) + $O_2(a^1\Delta_g)$, at 298 K, while region III (diagonal hatching) represents the contribution from the spin-forbidden process leading to O(^1D) formation via channel (R4), O(^1D) + $O_2(X^3\sum_g^-)$.

3.4. Quantum Yields at Wavelengths Shorter Than 305 nm

[30] For the wavelength range of 290–305 nm the value of 0.95 has been recommended by JPL 1997 [*DeMore et al.*, 1997] and JPL 2000 [*Sander et al.*, 2000]. However, two recent experimental studies reported by *Talukdar et al.* [1998] and *Taniguchi et al.* [2000] have indicated that the O(^1D) yield values in the wavelength range of 290–305 nm is ~0.90, using the standard point value of 0.79 at 308 nm. The yield values of *Trolier and Wiesenfeld* [1988] and *Ball et al.* [1997], which we renormalized above, also indicated values ~0.90. *Talukdar et al.* [1998] have reported the yield values do not depend on the temperature of O_3 in this wavelength range. The results of no dependence on the temperature can be explained by the small contribution of the hot-band excitation in this wavelength range, as will be described in section 4. The averaged value of the O(^1D) quantum yield is 0.90 over this wavelength range. Although it is likely that there is structure in the quantum yield spectrum in this wavelength range, the amplitude of the structure is <0.05. Therefore we recommend the yield of 0.90 in the range of 290–305 nm, which is independent of the temperature. The uncertainties of our recommended values in the 290 nm < λ < 305 nm range are estimated to be ±0.09.

[31] For the wavelength range of 220–290 nm the absolute yield at 248 nm is reported to be 0.91 ± 0.06 by *Talukdar et al.* [1998] and 0.94 ± 0.01 by *Greenblatt and Wiesenfeld* [1983], while the yield at 266 nm is 0.88 ± 0.02 by *Brock and Watson* [1980a]. The yield value in the wavelength range of 220–290 nm should be 0.85–0.95. However, the contribution from these wavelengths to O(^1D) production in the stratosphere and troposphere is not significant. Our understanding of ozone photochemistry would benefit from a better definition of the O(^1D) quantum yields in this region.

3.5. Quantum Yields at Wavelengths Longer Than 328 nm

[32] The O(^1D) quantum yield does not drop to 0 even at the wavelength longer than 328 nm. The formation of O(^1D) is attributed to the spin-forbidden dissociation to O(^1D) + $O_2(X^3\Sigma_g^-)$, (R4), as will be described in section 4. The energetic threshold for this spin-forbidden process (R4) is ~411 nm. This implies that the formation of O(^1D) can continue to 411 nm. *Bauer et al.* [2000] have measured the relative O(^1D) yield up to 370 nm. They have proposed the O(^1D) yield of 0.064 ± 0.006 between 325 and 375 nm. *Smith et al.* [2000] have reported the quantum yields are nearly constant (~0.12) and independent of temperature between 328 and 338 nm. In the wavelength range of 329–340 nm we recommend the value of 0.08±0.04, which is independent of the temperature. The $J(O^1D)$ value is still sensitive to the O(^1D) quantum yields around 330 nm at large solar zenith angles. Therefore more measurements are needed with various experimental techniques around 330–340 nm. The O(^1D) formation in the atmosphere above 340 nm is not significant owing to the small absorption coefficient of O_3.

3.6. Atmospheric Implications

[33] The recommendation for the quantum yield of O(^1D) in this work quantitatively includes the contributions of the photodissociation of vibrationally excited ozone and the spin-forbidden dissociation channel. For selected conditions (total ozone column of 300 Dobson units (DU), 298 K) we have compared the lower tropospheric photolysis frequencies, $J(O^1D)$, calculated using our recommendations and those by *DeMore et al.* [1994, 1997]. *DeMore et al.* [1994] did not account for the O(^1D) production from vibrationally excited ozone or from the spin-forbidden channel, and *DeMore et al.* [1997] did not account for the spin-forbidden channel. Using ground-based measurements of the solar actinic flux [*Hofzumahaus et al.*, 1999], we find that the photodissociation from vibrationally excited ozone contributes ~25–40% to the overall O(^1D) production rate for solar zenith angles from 40° to 80°, respectively. The contribution of the spin-forbidden channel is small at low solar zenith angles and reaches a value of ~30% at a solar zenith angle of 80°. These enhancements agree well with the model results reported for similar conditions by *Talukdar et al.* [1998], whose quantum yields are close to our data average (see Table 2). The $J(O^1D)$ values calculated using *Talukdar et al.*'s [1998] parameterization and our recommendations agree within 2% at ground and ambient temperature for all solar zenith angles up to 90°. In the upper troposphere and the lower stratosphere the relative impact of the spin-forbidden channel is much larger since it is temperature independent, whereas the contribution from the vibrationally excited ozone becomes less important at lower temperatures. A detailed discussion for these conditions can be found in the work by *Talukdar et al.* [1998], whose low-temperature quantum yields also agree well with the recommendation given in this work.

4. Formation Mechanisms of O(^1D) in the Photolysis of O_3

[34] There are five energetically possible fragmentation pathways in the UV/visible photolysis of O_3

$$O_3 + h\nu\ (\lambda < 310\ \text{nm}) \rightarrow \quad O(^1D) + O_2(a^1\Delta_g)$$

$$O_3 + h\nu\ (\lambda < 411\ \text{nm}) \rightarrow \quad O(^1D) + O_2(X^3\Sigma_g^-)$$

$$\text{(R7)} \qquad O_3 + h\nu\ (\lambda < 463\ \text{nm}) \quad \rightarrow \quad O(^3P) + O_2(b^1\Sigma_g^+)$$

$$\text{(R8)} \qquad O_3 + h\nu\ (\lambda < 612\ \text{nm}) \quad \rightarrow \quad O(^3P) + O_2(a^1\Delta_g)$$

$$\text{(R9)} \qquad O_3 + h\nu\ (\lambda < 1180\ \text{nm}) \rightarrow \quad O\left(^3P\right) + O_2(X^3\Sigma_g^-\Big),$$

where the long wavelength limits given in parentheses indicate the thermodynamic thresholds for the fragmentations at 298 K when the parent $O_3(X^1A_1)$ molecule is excited from its vibrationless level ($\nu'' = 0$) [*Atkinson et al.*, 1997]. For photodissociation in the Hartley band at λ < 300 nm it has generally been accepted that channels (R3) and (R9) are predominant, with reported quantum yields of ~0.9 and 0.1, respectively [*Adler-Golden et al.*, 1982]. The literature shows evidence for all the spin-forbidden channels, (R4), (R7), and (R8), as well as spin-allowed channels (R3) and (R9) occurring in the UV region above 300 nm, generally referred to as the Huggins band [*Wayne*, 1989]. Production of the O(^1D) atoms above 310 nm has been attributed to both channel (R3) via the photodissociation of internally excited O_3 and the spin-forbidden dissociation channel (R4) [*Adler-Golden et al.*, 1982; *Michelsen et al.*, 1994; *Takahashi et al.*, 1996a, 1996b, 1997, 1998a; *Silvente et al.*, 1997; *Ball et al.*, 1997; *Denzer et al.*, 1997, 1998; *Talukdar et al.*, 1998; *Bauer et al.*, 2000]. The contributions made by these excitation processes to the quantum yields for O(^1D) atoms from O_3 photolysis are schematically indicated in Figure 5. These excitation processes are schematically shown on an energy level diagram in Figure 6 and are now discussed in turn. This section shows the origin of the processes, which together lead to the complex variations of O(^1D) quantum yield as a function of wavelength and temperature. This discussion also justifies, to first order, the expression for the quantum yield that is adopted in this evaluation.

[35] The transition responsible for the Hartley band takes the molecule from its ground X^1A_1 state to an electronically excited $^1B_2$ state [*Wayne*, 1989], and the angular distribution of the fragments is consistent with this being a mainly parallel dissociation (the transition dipole moment lying in the molecular plane and perpendicular to the C_{2v} axis), with dissociation of the bent O_3 molecule dominantly in (R3) being rapid in comparison with molecular rotation [*Fairchild et al.*, 1978; *Suits et al.*, 1993; *Thelen et al.*, 1995; *Blunt and Suits*, 1997; *Takahashi et al.*, 1998b; *Hancock et*

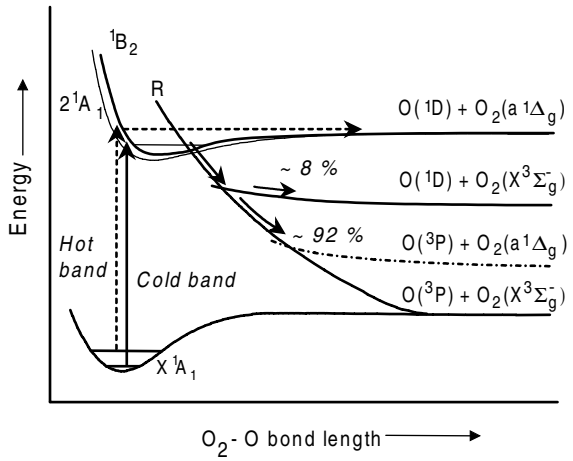

Figure 6. Schematic diagram of the potential curves as a function of dissociation coordinate with the possible dissociation channels indicated. The energies of the vibrationally excited molecule are not shown to scale and serve to illustrate excitation to form O(^1D) and $O_2(a^1\Delta_g)$ products from hot-band excitation at photon energies where the process is energetically forbidden for the ground vibrational state.

al., 1999]. The origin of the structured part of the Huggins band at wavelengths above ~310 nm, however, has been the subject of some debate. Transitions are seen which support vibrational structure, but no distinct rotational lines can be observed, and the electronic parentage has been assigned as transitions to the same $^1B_2$ state as for the Hartley band, which supports bound vibrational levels below the threshold to process (R3) [*Katayama*, 1979] or to bound vibrational levels of a $^1A_1$ state reached in a two-electron transition from the ground $^1A_1$ (0, 0, 0) state but with an odd quantum number change in the antisymmetric stretch mode ν_3, making the overall symmetry $^1B_2$ [*Joens*, 1994] and presumably gaining intensity from the nearby one-photon $^1B_2$ state. Measurements of the rotational contours of the Huggins bands have been carried out [*Sinha et al.*, 1986; *Takahashi et al.*, 1997], with the most recent measurements favoring the rotational constants which are calculated for the second $^1A_1$ state [*Takahashi et al.*, 1997]. Translational anisotropy measurements are unable to distinguish the two possibilities but are consistent with both, as positive values of the translational anisotropy factor β are both predicted and measured [*Denzer et al.*, 1997, 1998; *Hancock et al.*, 1999].

4.1. Photolysis of Internally Excited Ozone

[36] The most recent experimental approach to determine the bond energy for the dissociation of jet-cooled O_3 into O(^1D) + $O_2(a^1\Delta_g)$ yields a value of 386.59 ± 0.04 k J mol^{-1}, and the standard heat of formation of O_3 at 0 K is calculated to be $\Delta_f H^0(O_3) = -144.31 \pm 0.14$ k J mol^{-1} [*Taniguchi et al.*, 1999]. This corresponds to a wavelength limit at 0 K of 309.44 ± 0.02 nm for channel (R3). Formation of the O(^1D) atoms at $\lambda > 309.45$ nm, however, was observed in the flow cell experiments at 200–320 K, and we attribute the temperature-dependent part of the quantum yield to the photodissociation of vibrationally excited parent O_3. The energy difference in the threshold energies for the cold and hot bands was measured to be 1056 ± 20 cm^{-1} from the difference in the threshold photolysis wavelengths [*Takahashi et al.*, 1997]. The vibrational spacing for the antisymmetric stretching ν_3 vibration of $O_3(X^1A_1)$, 1042 cm^{-1} [*Barbe et al.*, 1974], is equal to this difference within experimental error (the ν_1 and ν_2 levels are at 1103 and 701 cm^{-1}), and therefore the active vibrational mode in the hot-band excitation is assigned to the antisymmetric vibration. The thermal population in the $\nu_3'' = 1$ level of $O_3(X^1A_1)$ is calculated to be only 0.6% of that of the $\nu'' = 0$ level at room temperature, but the Franck-Condon factor for the vibrational transition is suggested to several tens of times or more; larger for the $\nu_3'' = 1$ level than for the $\nu'' = 0$ level because of preferential overlap of the potential surfaces of the ground and excited states [*Michelsen et al.*, 1994; *Taniguchi et al.*, 2000]. The influences of population in the other vibrational states (ν_1 symmetric stretch and ν_2 bending) are not known because of a lack of detailed Franck-Condon factors for the possible transitions, although the experimental evidence clearly shows the importance of the ν_3 level. Thus the contribution of the hot band is nonnegligible in the near-UV region.

4.2. Spin-Forbidden Processes

[37] In the Huggins band region, there is clear evidence for the existence of a spin-forbidden channel forming O(^1D). Measurements of the translational energy distributions of the O(^1D) fragments have shown that they contain contributions from species formed with kinetic energies well above those possible on energetic grounds from process (R3) and are entirely consistent with those expected from process (R4) [*Takahashi et al.*, 1996b; *Denzer et al.*, 1997, 1998]. We attribute the temperature-independent part of the quantum yield above 320 nm to this process. At shorter wavelengths it can still be distinguished from the spin-allowed step; photofragment spectroscopy experiments have shown it to be observable at 313 nm [*Denzer et al.*, 1998], and the approximate constancy of the quantum yield for the lowest temperature data above 313 nm suggests that there is a persistent spin-forbidden yield at about the 8–9% level above this wavelength at all temperatures. There is no evidence at present for a contribution of this magnitude at shorter wavelengths, where only the spin-allowed processes (R3) and (R9) have been observed.

[38] We now consider the parentage of the spin-forbidden products. The assignments of both *Joens* [1994] and *Katayama* [1979] suggest that the initial absorption in the structured region is to a singlet state, so that absorption would be followed by a curve crossing to a dissociative triplet state. Lifetimes of the states reached by absorption in the structured bands are seen to increase with increasing wavelength in measurements of both line widths [*Takahashi et al.*, 1997] and translational anisotropies [*Hancock et al.*, 1999]. This observation is consistent with an energy-dependent intersystem crossing rate and would not be expected for direct absorption to a dissociative triplet state. Thus we favor singlet to triplet crossing following spin-allowed absorption in this region, although we cannot rule out a contribution from any (as yet unassigned) singlet to triplet absorption.

[39] Measurements of Doppler widths [*Takahashi et al.*, 1996b] and translational energies [*Denzer et al.*, 1998] have shown that the ratio of spin-allowed to spin-forbidden O(^1D) formation is smaller on peaks in the Huggins band than in the troughs between them. If absorption on the peaks has a marked component that corresponds to transitions to bound levels of an upper singlet state which then predissociates to form channels other than process (R3)(including formation of ground state O(^3P) atoms), whereas absorption in the troughs has a relatively larger component from the hot bands of ozone, then there is a possibility of the O(^1D) quantum yield showing some structure. Furthermore, as the absorption peaks become more pronounced at lower temperatures, any structure may be temperature dependent. Only one set of quantum yield data, that of *Takahashi et al.* [1996a, 1998a], shows continuous measurements over the structured region; all other data are taken at specific wavelengths. Their room temperature measurements show the photofragment yield spectrum of O(^1D) to be virtually structure free between 310 and 325 nm, and thus the quantum yield shows a small anticorrelation with the absorption spectrum [*Takahashi et al.*, 1996a, 1998a]. At low temperatures above 320 nm, there is slight structure on the photofragment yield spectrum which correlates with that in absorption [*Takahashi et al.*, 1998a], and results at longer wavelengths show that the photofragment yield follows closely the absorption spectrum [*Bauer et al.*, 2000]. The effect on

the O(^1D) yield of taking into account any local variations in the tail will be small in comparison with the change brought about by the new recommendations but would warrant further investigation.

5. Summary

[40] To rectify the lack of a good recommendation for the quantum yields for O(^1D) in ozone photolysis, the panel of the scientists working in the area of ozone photodissociation has critically evaluated the data available to date and developed the best possible data set for atmospheric modeling. The experimental techniques used in the experiments of O(^1D) quantum yield measurements were reviewed. The quantum yield of O(^1D) at 298 K at 308 nm was set to 0.79 on the basis of absolute quantum yield measurement studies. The wavelength dependence of quantum yields at 298 K between 306 and 328 nm was derived by checking and renormalizing the recent experimental data presented by the eight groups and then averaging them. The wavelength dependence at 298 K was anchored at 308 nm. The comprehensive, easy-to-use equation (3)was employed for 306 nm $< \lambda <$ 328 nm and 200 K $< T <$ 320 K by fitting the experimental data of the temperature dependence as well as the yields at 298 K obtained above to (3). The recommendation for the quantum yield of O(^1D) in this work quantitatively includes the contributions of the hot-band excitation and the spin-forbidden dissociation channel. These contributions significantly affect estimations of the O(^1D) production rate in the troposphere and stratosphere.

[41] **Acknowledgments.** This work was partly supported by International Joint Research grants of the New Energy and Industrial Technology Development Organization (NEDO). A.R.R. thanks NOAA's Climate and Global change program and NASA's Upper Atmospheric Research program for financial support. This work was carried out as a part of the SPARC (WCRP)/IGAC (IGBP) joint activity on laboratory studies. A.J.H. acknowledges the support of the National Science Foundation through grants ATM-9625437 and ATM0002242. A.H. and G.H. thank the Commission of the European Communities for financial support through the EC Environment Programme. We thank Mary Gilles (NOAA/AL) for her intercomparison work of the power meters and discussions about the results.

References

Adler-Golden, S. M., E. L. Schweitzer, and J. I. Steinfeld, Ultraviolet continuum spectroscopy of vibrationally excited ozone, *J. Chem. Phys.*, *76*, 2201–2209, 1982.

Ahmed, M., E. R. Wouters, D. S. Peterka, O. S. Vasyutinskii, and A. G. Suits, Atomic orbital alignment and coherence in N_2O photodissociation at 193.3 nm, *Faraday Discuss.*, *113*, 425–436, 1999.

Amimoto, S. T., A. P. Force, J. R. Wiesenfeld, and R. H. Young, Direct observation of O(^3P_j) in the photolysis of O_3 at 248 nm, *J. Chem. Phys.*, *73*, 1244–1247, 1980.

Armerding, W., F. J. Comes, and B. Schülke, O(^1D) quantum yield of ozone photolysis in the UV from 300 nm to its threshold and at 355 nm, *J. Phys. Chem.*, *99*, 3137–3143, 1995.

Arnold, I., F. J. Comes, and G. K. Moortgat, Laser flash photolysis: Quantum yield of O(^1D) formation from ozone, *Chem. Phys.*, *24*, 211–217, 1977.

Atkinson, R., D. L. Baulch, R. A. Cox, R. F. Hampson, Jr., J. A. Kerr, M. J. Rossi, and J. Troe, Evaluated kinetic and photochemical data for atmospheric chemistry: Supplement VI, in *IUPAC Sub-committee on Gas Kinetic Data Evaluation for Atmospheric Chemistry*, *J. Phys. Chem. Ref. Data.*, *26*, 1329–1500, 1997.

Ball, S. M., G. Hancock, I. J. Murphy, and S. P. Rayner, Ray, The relative quantum yields of $O_2(a^1\Delta_g)$ from the photolysis of ozone in the wavelength range 270 nm $< \lambda <$ 329 nm, *Geophys. Res. Lett.*, *20*, 2063–2066, 1993.

Ball, S. M., G. Hancock, S. E. Martin, and J. C. Pinot de Moira, A direct measurement of the O(^1D) quantum yields from the photodissociation of ozone between 300 and 328 nm, *Chem. Phys. Lett.*, *264*, 531–538, 1997.

Barbe, A., C. Secroun, and P. Jouve, Infrared spectra of $^{16}O_3$ and $^{18}O_3$: Darling and Dennison resonance and anharmonic potential function of ozone, *J. Mol. Spectrosc.*, *49*, 171–182, 1974.

Bauer, D., L. D'Ottone, and A. J. Hynes, O ^1D quantum yields from O_3 photolysis in the near UV region between 305 and 375 nm, *Phys. Chem. Chem. Phys.*, *2*, 1421–1424, 2000.

Blunt, D. A., and A. G. Suits, Photodissociation of Ozone at 276 nm by photofragment imaging and high-resolution photofragment translational spectroscopy, *ACS Symp. Ser.*, *678*, 99–106, 1997.

Brock, J. C., and R. T. Watson, Ozone photolysis: Determination of the O(^3P) quantum yield at 266 nm, *Chem. Phys. Lett.*, *71*, 371–375, 1980a.

Brock, J. C., and R. T. Watson, Laser flash photolysis of ozone: O(^1D) quantum yields in the fall-off region 297–325 nm, *Chem. Phys.*, *71*, 477–484, 1980b.

Cooper, I. A., P. J. Niel, and J. R. Wiesenfeld, Relative quantum yield of O($^1D_2$) following ozone photolysis between 221 and 243.5 nm, *J. Geophys. Res.*, *98*, 12,795–12,800, 1993.

DeMore, W. P., S. P. Sander, C. J. Howard, A. R. Ravishankara, D. M. Golden, C. E. Kolb, R. F. Hampson, M. J. Kurylo, and M. J. Molina, Chemical kinetics and photochemical data for use in stratospheric modeling, *JPL Publ.*, *94–26*, 1994.

DeMore, W. P., S. P. Sander, C. J. Howard, A. R. Ravishankara, D. M. Golden, C. E. Kolb, R. F. Hampson, M. J. Kurylo, and M. J. Molina, Chemical kinetics and photochemical data for use in stratospheric modeling, *JPL Publ.*, *97–104*, 1997.

Denzer, W., G. Hancock, J. C. Pinot de Moira, and P. L. Tyley, Direct observation of spin-forbidden formation of O(^1D) in the near-UV photolysis of ozone, *Chem. Phys. Lett.*, *280*, 496–500, 1997.

Denzer, W., G. Hancock, J. C. Pinot de Moira, and P. L. Tyley, Spin-forbidden dissociation of ozone in the Huggins bands, *Chem. Phys.*, *231*, 109–120, 1998.

Fairchild, C. E., E. J. Stone, and G. M. Lawrence, Photofragment spectroscopy of ozone in the UV region 270–310 nm and at 600 nm, *J. Chem. Phys.*, *69*, 3632–3638, 1978.

Fairchild, P. W., and E. K. C. Lee, Relative quantum yield of O(^1D) in ozone photolysis in the region between 250 and 300 nm, *Chem. Phys. Lett.*, *60*, 36–39, 1978.

Greenblatt, G. D., and J. R. Wiesenfeld, Time-resolved resonance fluorescence studies of O($^1D_2$) yields in the photodissociation of O_3 at 248 and 308 nm, *J. Chem. Phys.*, *78*, 4924–4928, 1983.

Hancock, G., and A. Hofzumahaus, Experimental study of the altitude dependence of the tropospheric ozone photolysis frequency J(O^1D) between 0 and 12 km height (ATOP), *Eur. Res. and Dev. Prog. Environ. and Clim. Rep. ENV4-CT95-0158*, Forsch. Juelich, Juelich, Germany, 1997.

Hancock, G., R. D. Johnson, J. C. Pinot de Moira, G. A. D. Ritchie, and P. L. Tyley, The photodissociation dynamics of tropospheric ozone, in *Advances in Atomic and Molecular Beams*, edited by R. Campargue, pp. 331–342, Springer-Verlag, New York, 1999.

Heidner, R. F., III, and D. Husain, Quenching of O($^1D_2$) by atmospheric gases, *Nature*, *241*, 10–11, 1973.

Hofzumahaus, A., A. Kraus, and M. Müller, Solar actinic flux spectroradiometry: A technique for measuring photolysis frequencies in the atmosphere, *Appl. Opt.*, *38*, 4443–4460, 1999.

Joens, J. A., Reassignment of the vibrational structure of the Huggins absorption band of ozone, *J. Chem. Phys.*, *101*, 5431–5437, 1994.

Katayama, D. H., New vibrational quantum number assignments for the UV absorption bands of ozone based on the isotope effect, *J. Chem. Phys.*, *71*, 815–820, 1979.

Kuis, S., R. Simonaitis, and J. Heicklen, Temperature dependence of the photolysis of ozone at 3130 Å, *J. Geophys. Res.*, *80*, 1328–1331, 1975.

Malicet, J., D. Daumont, J. Charbonnier, C. Parisse, A. Chakir, and J. Brion, Ozone UV spectroscopy, II, Absorption cross-sections and temperature dependence, *J. Atmos. Chem.*, *21*, 263–273, 1995.

Michelsen, H. A., R. J. Salawitch, P. O. Wennberg, and J. G. Anderson, Production of O(^1D) from photolysis of O_3, *Geophys. Res. Lett.*, *21*, 2227–2230, 1994.

Molina, L. T., and M. J. Molina, Absolute absorption cross sections of ozone in the 185- to 350-nm wavelength range, *J. Geophys. Res.*, *91*, 14,501–14,508, 1986.

Moortgat, G. K., and P. Warneck, Relative O(^1D) quantum yields in the near UV photolysis of ozone at 298 K, *Z. Naturforsch.*, *30A*, 835–844, 1975.

Müller, M. A., A. Kraus, and A. Hofzumahaus, $O_3 \rightarrow$ O(^1D) photolysis frequencies determined from spectroradiometric measurements of solar actinic UV-radiation: Comparison with chemical actinometer measurements, *Geophys. Res. Lett.*, *22*, 679–682, 1995.

Neyer, D. W., A. J. R. Heck, D. W. Chandler, J. M. Teule, and M. H. M. Janssen, Speed-dependent alignment and angular distributions of O($^1D_2$) from the ultraviolet photodissociation of N_2O, *J. Phys. Chem.*, *103*, 10,388–10,397, 1999.

Philen, D. L., R. T. Watson, and D. D. Davis, A quantum yield determination of O(^1D) production from ozone via laser flash photolysis, *J. Chem. Phys.*, *67*, 3316–3321, 1977.

Pratt, S. T., P. M. Dehmer, and J. L. Dehmer, Photoionization of an autoionizing level of atomic oxygen, *Phys. Rev. A*, *43*, 282–285, 1991.

Ravishankara, A. R., G. Hancock, M. Kawasaki, and Y. Matsumi, Atmospheric photochemistry of ozone: Surprises and recent lessons, *Science*, *280*, 60–61, 1998.

Richter, R. C., and A. J. Hynes, Direct detection of oxygen $^1D_2$ atoms by mass-resolved, resonance-enhanced multiphoton ionization spectroscopy, following ozone photolysis at ~276 nm, *J. Phys. Chem.*, *100*, 8061–8063, 1996.

Sander, S. P., et al., Chemical kinetics and photochemical data for use in stratospheric modeling, *JPL Publ.*, *00-3*, 2000.

Shetter, R. E., et al., Actinometric and radiometric measurement and modeling of the photolysis rate coefficient of ozone to O(^1D) during Mauna Loa Observatory Photochemistry, Experiment 2 O(^1D), *J. Geophys. Res.*, *101*, 14,631–14,641, 1996.

Silvente, E., R. C. Richter, M. Zheng, E. S. Salzman, and A. J. Hynes, Relative quantum yields for O^1D production in the photolysis of ozone between 301 and 336 nm: Evidence for the participation of a spin-forbidden channel, *Chem. Phys. Lett.*, *264*, 309–315, 1997.

Sinha, A., D. Imre, J. H. Goble, Jr., and J. L. Kinsey, Excitation spectroscopy of jet-cooled ozone: The Huggins system, *J. Chem. Phys.*, *84*, 6108–6114, 1986.

Smith, G. D., L. T. Molina, and M. J. Molina, Temperature dependence of O(^1D) quantum yields from the photolysis of ozone between 295 and 338 nm, *J. Phys. Chem.*, *104*, 8916–8921, 2000.

Steinfeld, J. I., S. M. Adler-Golden, and J. W. Gallagher, Critical survey of data on the spectroscopy and kinetics of ozone in the mesosphere and thermosphere, *J. Phys. Chem. Ref. Data.*, *16*, 911–951, 1987.

Suits, A. G., R. L. Miller, L. S. Bontuyan, and P. L. Houston, Photofragment vector correlations by ion imaging: $O_2(a^1\Delta_g(v, J))$ from 248 nm dissociation of ozone, *J. Chem. Soc. Faraday Trans.*, *89*, 1443–1448, 1993.

Suzuki, T., H. Katagiri, Y. Mo, and K. Tonokura, Evidence for multiple dissociation components and orbital alignment in 205 nm photodissociation of N_2O, *Chem. Phys. Lett.*, *256*, 90–95, 1996.

Takahashi, K., Y. Matsumi, and M. Kawasaki, Photodissociation processes of ozone in the Huggins band at 308-326 nm: Direct observation of O($^1D_2$) and O(^3P_j) products, *J. Phys. Chem.*, *100*, 4084–4089, 1996a.

Takahashi, K., M. Kishigami, Y. Matsumi, M. Kawasaki, and A. J. Orr-Ewing, Observation of the spin-forbidden O(^1D) + $O_2(X^3\Sigma_g^-)$ channel in the 317–327 nm photolysis of ozone, *J. Chem. Phys.*, *105*, 5290–5293, 1996b.

Takahashi, K., M. Kishigami, N. Taniguchi, Y. Matsumi, and M. Kawasaki, Photofragment excitation spectrum for O(^1D) from the photodissociation of jet-cooled ozone in the wavelength range 305–329 nm, *J. Chem. Phys.*, *106*, 6390–6397, 1997.

Takahashi, K., N. Taniguchi, Y. Matsumi, M. Kawasaki, and M. N. R. Ashfold, Wavelength and temperature dependence of the absolute O(^1D) yield from the 305–329 nm photodissociation of ozone, *J. Chem. Phys.*, *108*, 7161–7172, 1998a.

Takahashi, K., N. Taniguchi, Y. Matsumi, and M. Kawasaki, Translational energy and angular distributions of O(^1D) and O(^3P_j) fragments in the UV photodissociation of ozone, *Chem. Phys.*, *231*, 171–182, 1998b.

Talukdar, R. K., M. K. Gilles, F. Battin-Leclerc, and A. R. Ravishankara, Photolysis of ozone at 308 and 248 nm: Quantum yield of O(^1D) as a function of temperature, *Geophys. Res. Lett.*, *24*, 1091–1094, 1997.

Talukdar, R. K., C. A. Longfellow, M. K. Gilles, and A. R. Ravishankara, Quantum yields of O(^1D) in the photolysis of ozone between 289 and 329 nm as a function of temperature, *Geophys. Res. Lett.*, *25*, 143–146, 1998.

Taniguchi, N., K. Takahashi, Y. Matsumi, S. M. Dylewski, J. D. Geiser, and P. L. Houston, Determination of the heat of formation of O_3 using vacuum ultraviolet laser-induced fluorescence spectroscopy and two-dimensional product imaging techniques, *J. Chem. Phys.*, *111*, 6350–6355, 1999.

Taniguchi, N., K. Takahashi, and Y. Matsumi, Photodissociation of O_3 around 309 nm, *J. Phys. Chem.*, *104*, 8936–8944, 2000.

Thelen, M. A., T. Gejo, J. A. Harrison, and J. R. Huber, Photodissociation of ozone in the Hartley band: Fluctuation of the vibrational state distribution in the $O_2(^1\Delta_g)$ fragment, *J. Chem. Phys.*, *103*, 7946–7955, 1995.

Trolier, M., and J. R. Wiesenfeld, Relative quantum yield of O($^1D_2$) following ozone photolysis between 275 and 325 nm, *J. Geophys. Res.*, *93*, 7119–7124, 1988.

Wayne, R. P., The photochemistry of ozone, in *The Handbook of Environmental Chemistry,* vol. 2, part E, edited by O. Hutzinger, pp. 1–56, Springer-Verlag, New York, 1989.

F. J. Comes, Johann Wolfgang Goethe Universität, Institut für Physikalische und Theoretische Chemie, Marie-Curie-Strasse 11, D-60439 Frankfurt, Germany. (comes@chemie.uni-frankfurt.de)

G. Hancock, Physical and Theoretical Chemistry Laboratory, Oxford University, South Parks Road, Oxford OX1 3QZ, England, UK. (gus.hancock@chemistry.ox.ac.uk)

A. Hofzumahaus, Institut für Chemie und Dynamik der Geosphäre, Institut II: Troposphäre, Forschungszentrum Jülich GmbH, Leo Brandtstrasse, D-52425 Jülich, Germany. (a.hofzumahaus@fz-juelich.de)

A. J. Hynes, Division of Marine and Atmospheric Chemistry, RSMAS, University of Miami, 4600 Rickenbacker Causeway, Miami, FL 33149, USA. (ahynes@rsmas.miami.edu)

M. Kawasaki, Department of Molecular Engineering, Kyoto University, Kyoto 606-8501, Japan. (mkawasa7@ip.media.kyoto-u.ac.jp)

Y. Matsumi, Solar-Terrestrial Environment Laboratory, Nagoya University, Honohara 3-13, Nagoya 442-8507, Japan. (matsumi@stelab.nagoya-u.ac.jp)

A. R. Ravishankara, Aeronomy Laboratory, NOAA, R/E/AL, 325 Broadway, Boulder, CO 80305, USA. (ravi@al.noaa.gov)